Double photoexcitation involving $2p$ and $4f$ electrons in L_3-edge x-ray absorption spectra of protactinium

Christoph Hennig
Forschungszentrum Dresden-Rossendorf, Institute of Radiochemistry, D-01314 Dresden, Germany

Claire Le Naour
CNRS/Université Paris-Sud, Institut de Physique Nucléaire, 91406 Orsay Cedex, France

Christophe Den Auwer
CEA Marcoule, DEN/DRCP/SCPS, 30207 Bagnols sur Cèze Cedex, France

(Received 11 April 2008; revised manuscript received 7 May 2008; published 3 June 2008)

The L_3-edge x-ray absorption spectrum of Pa(V) fluoride in aqueous solution show clear evidence for the double photoexcitation involving $2p$ and $4f$ electrons. A comparison with the $[2p4f]$ double-electron excitations observed in the L_3-edge x-ray absorption spectra of other actinides (thorium, uranium, neptunium, plutonium, and americium) indicates a monotonic increase in the excitation energy. The sharp edgelike structure of the multielectron excitation reveals the origin of a shake-up channel.

DOI: 10.1103/PhysRevB.77.235102 PACS number(s): 78.70.Dm

I. INTRODUCTION

Sensitive measurements of the x-ray absorption cross section reveal that above the absorption edge, often weak additional resonance peaks occur related to multielectron photoexcitations. Early studies of these spectral features have been performed on noble gases[1–3] because their absorption spectra are not affected by the photoelectron backscattering effect of coordinated atoms, known as extended x-ray absorption fine structure (EXAFS). In many other cases it was possible to suppress the single-electron backscattering fine structure by vaporizing chemical elements to obtain monoatomic gases.[4,5] On the other hand, multielectron resonances have been extracted also from absorption spectra in presence of neighboring atoms which generate a mixed signal between multielectron excitation and EXAFS.[6] Two types of multielectron excitation have been identified: (i) sharp thresholdlike features, superimposed onto the photoelectron backscattering signal, could be indicated as shake-up transitions; and (ii) shake-off transitions were recognized as a change in the slope of the absorption signal.[7] The $[2p(2s)4f]$ excitation energy for the early elements in the sixth period ($Z \leq 79$) is less than 100 eV above the corresponding L edges. Several studies have been performed to reveal the $[2p(2s)4f]$ energy of the elements $Z=79-83$ (Refs. 8–10). A detailed discussion of these elements in different oxidation states was provided by Di Cicco and Filipponi,[9] indicating the $[2p4f]$ energy for Hg (135 ± 5 eV), Pb (180 ± 10 eV), and Bi (200 ± 10 eV). Theoretical predictions of the $[2p4f]$ and $[2s4f]$ double-electron excitation energies proposed for up to radon ($Z=86$) shows a monotonic increase with the atomic number Z.[11] However, elements with $Z \geq 84$ comprise only radioactive isotopes and the measurements require therefore specific radiation protection. A simultaneous excitation of $2p$ and $4f$ electrons, visible in the L-edge spectra of actinides, generates LN-edge double-electron excitations.[12] The early actinides Th, U, Np, Pu, and Am show a systematic shift in the $[2p4f]$ energies ($L_3N_{6,7}$ in absorption edge notation). However, the $[2p4f]$ double-electron excitation energy of protactinium has not been estimated up to now. The aim of this paper is therefore to prepare a protactinium sample which is appropriate to extract the double-electron feature and to determine its excitation energy.

Protactinium is a rare element. It occurs with a Pa/U ratio of 3.2×10^{-7} in undisturbed uranium ore as a product of the radioactive decay of uranium.[13] Natural weathering and leaching of the uranium ore result in an intermediate enrichment of Pa in sea water followed by hydrolysis and deposition in ocean sediment. The enrichment of Pa has been used to determine the age of marine sediments.[14,15] Natural uranium consists of the primordial uranium isotopes ^{238}U (99.275%), ^{235}U (0.720%), as well as ^{234}U (0.005%), the decay product of ^{238}U. The isotope ^{234}Pa is a decay product of ^{238}U according to the decay reaction

$$^{238}_{92}\mathrm{U} \xrightarrow{\alpha} {}^{234}_{90}\mathrm{Th} \xrightarrow{\beta^-} {}^{234m}_{91}\mathrm{Pa} \xrightarrow{\beta^-} {}^{234}_{92}\mathrm{U}. \quad (1)$$

This protactinium isotope occurs in two nuclear isomeric forms: the ground state ^{234}Pa and the metastable, but long-lived, excited state ^{234m}Pa. Protactinium was first identified in 1913 as ^{234m}Pa by Fajans and Göhring,[16] and ^{234}Pa was discovered in 1921 by Hahn.[17] Only 0.13% of metastable ^{234m}Pa decays in the ground state, generating ^{234}Pa before both decaying to ^{234}U. Because its half-life is only 1.17 min, the use of ^{234m}Pa it is not appropriate for the present long-term experiments. Among the known protactinium isotopes, ^{231}Pa is the most stable one with a half-life of 3.276×10^4 yr. This isotope is formed by the alpha decay of ^{235}U followed by the beta decay of ^{231}Th:

$$^{235}_{92}\mathrm{U} \xrightarrow{\alpha} {}^{231}_{90}\mathrm{Th} \xrightarrow{\beta^-} {}^{231}_{91}\mathrm{Pa} \xrightarrow{\alpha} {}^{227}_{89}\mathrm{Ac}. \quad (2)$$

^{231}Pa was first discovered in 1918 by Hahn and Meitner[18] and simultaneously by Soddy and Cranston.[19] The primary decay mode of ^{231}Pa and lighter isotopes is a decay to actinium isotopes, whereas the heavier Pa isotopes undergo a

β^- decay to uranium isotopes. Protactinium is related to an extraordinary chemistry due to its position at the beginning of the actinide series, whose chemical properties depend on the delocalized $5f$ and $6d$ electron configuration. The participation of $5f$ orbitals of Pa(V) to the bonding with fluorine has been found necessary to explain the structure of Na_3PaF_8, wherein the Pa atom lies in the center of an almost perfect cube.[20] In aqueous solution, the two oxidation states Pa(IV) and Pa(V) have been established. Pa(V) is stable under oxic conditions in solutions. The instability of Pa(IV) toward reoxidation complicates the conservation of the pure oxidation state. The existence of lower oxidation states has been deduced from cocrystallization of protactinium at tracer scale with a bivalent lanthanide in chloride melts;[21] whereas in the solid state, the thermal decomposition of PaI_5 could lead to the formation of $Pa^{III}I_3$.[22] Pa(IV) can be identified by Laporte allowed $5f^1 \rightarrow 6d^1$ transitions, leading to the observation of three absorption bands (~230, ~260, and ~280 nm), whose positions and widths vary slightly with the medium. On the other hand, Pa(V) spectra exhibit a strong absorption in the UV range (~210 nm) that has been related to either an electron transfer from the ligand to the metal or to the occurrence of an oxo bond. However, effects from the solvent medium should be considered.[23–25] The coordination chemistry of Pa(IV) is similar to the next higher actinides, whereas Pa(V) shows a unique coordination behavior. The next higher actinides, U, Np, Pu, and Am, generate in the oxidation state V actinyl ions with two strongly covalent oxo groups, AnO_2^+, having the character of a triple bond.[26] In contrast, Pa(V) has either only one mono-oxo bond or no oxo bond, depending on the coordinating ligands.[27] The formation of the mono-oxo protactinyl cation PaO^{3+} is preferred over that of PaO_2^+ because the $6d$ orbitals of Pa(V) destabilize the π orbitals of PaO_2^+ due to conflicting $6d$-$2p$ antibonding orbitals.[28]

II. EXPERIMENTAL DETAILS

A. Sample preparation

For this experiment, the protactinium isotope ^{231}Pa from the IPN Orsay stock has been used. The decay products ^{223}Ra, ^{227}Ac, and ^{227}Th were removed from the solution by anion exchange using AG-MP1 resin (Bio-Rad) according to the procedure described in Ref. 27. 20 mg ^{231}Pa was dissolved in 10M HCl and percolated onto the anion exchange column. Under these conditions, Pa was retained on the resin; whereas Ra, Ac, and Th passed through. In the next step, Pa was eluted from the column with 0.1M HF/8M HCl. The eluted Pa fraction was evaporated to dryness, and the residue was taken up in concentrated HCl. This procedure was repeated six times; and finally, the residue was taken up in 0.05M HF. The quantitative ^{231}Pa amount was determined by gamma spectroscopy. The spectrum showed the characteristic emission lines of ^{231}Pa at 283.67, 300.08, 302.07, and 330.07 keV and only a negligible contribution from ^{227}Th and ^{223}Ra impurities. The sample for the EXAFS measurement consisted of 1.0×10^{-3} Pa(V) in aqueous solution with 5×10^{-2} HF. The UV-visible measurement (Shimadzu 3101) showed the typical spectrum of Pa(V) in this medium: a high absorption at low wavelengths, followed by a monotonous decrease in the absorbance with increasing wavelength.

B. X-ray absorption spectroscopy data acquisition and treatment

X-ray absorption measurements were performed at room temperature on the solution in a 200 μL cell specifically designed for radioactive samples. The measurements were carried out at the Rossendorf Beamline[29] (ROBL) at ESRF (6.0 GeV, 200 mA) in transmission mode with a water-cooled double-crystal Si(111) monochromator. The Rossendorf Beamline is constructed according to the requirements of handling radioactive materials, including a glove box to protect the experimentalists against radionuclide release. The sample was encapsulated in double confinement. A constant intensity of the primary beam, I_0, was achieved by detuning the second crystal using a piezosystem with a feedback loop referring to 70% of the incoming beam intensity I_0. The intensity was taken constant over the whole spectrum in the range of $\pm 0.04\%$ of I_0. Multiple diffraction peaks from the monochromator (glitches) were rejected by this system. Two Pt coated mirrors were used in total reflection mode. The first mirror collimated the x-ray beam onto the first monochromator crystal; the second mirror focused the beam vertically to the sample. Higher harmonics in the monochromatic beam were rejected by this mirror arrangement. The energy was calibrated according to the K edge of an yttrium metal foil by using the first inflection point of the absorption edge at 17 038.0 eV. The XAFS data were extracted from the raw data by subtracting a polynomial function, which was fitted to the pre-edge region. Subsequently, the atomic background above the absorption edge, $\mu_0(E)$, was approximated by a spline function. The fine structure $\chi(E)$ was obtained from the raw data $\mu(E)$ by using $\chi(E)=[\mu(E)-\mu_0(E)]/\ \mu_0(E)]$, converted to $\chi(k)$ and weighted with k^3. Data extraction and EXAFS fits were performed using the WINXAS[30] and EXAFSPAK[31] software. The EXAFS data were fitted using theoretical phase and amplitude functions calculated with the FEFF 8.2 code[32] from K_2PaF_7. The fine structure of the multielectron transition was separated from the signal by subtracting the data of EXAFS shell fit from the experimental data $\chi(E)$.

III. RESULTS AND DISCUSSION

A. Extended x-ray absorption fine structure background signal

The extraction of multielectron effects requires an absorption spectrum which is in an ideal case free from backscattering effects of neighboring atoms as in monoatomic gases. Vaporization, as can be applied for some lighter elements, is complicated for very heavy elements especially due to the low vapor pressure and difficulties due to radioprotection conditions. An alternative is the use of protactinium in aqueous solution. In there it is coordinated by light ligands, resulting in only comparable weak backscattering signal from neighboring atoms. On the other hand, aqueous protactinium shows a complicated solution chemistry because it undergoes

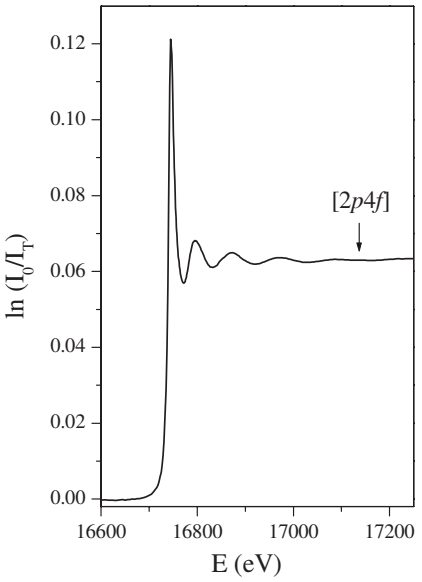

FIG. 1. Pa L_3-absorption edge corrected for the atomic background in the pre-edge region. The arrows indicate the expected energy E_f of the $[2p4f]$ double-electron excitation.

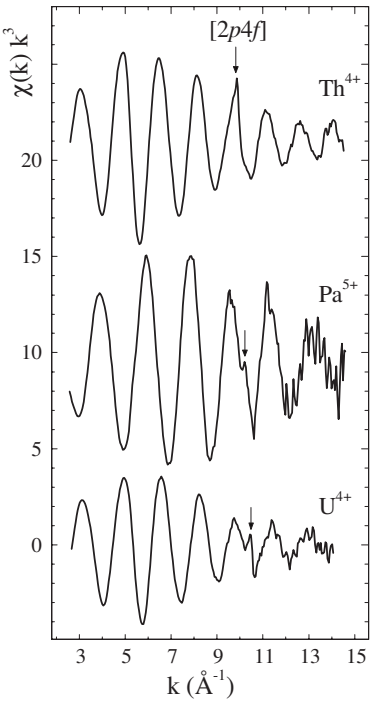

FIG. 2. Experimental k^3-weighted extended x-ray absorption fine structure at the L_3 edges of Th^{4+}, Pa^{5+}, and U^{4+} solutions. The arrows indicate the maxima of the $[2p4f]$ double-electron excitations. The energy of the feature in the spectrum of Pa^{5+} is given as E_f in Table II. The spectra of Th^{4+} and U^{4+} are taken from Ref. 12.

easy hydrolysis and polymerization reactions followed by precipitation.[33] This occurs also in $HClO_4$ and HNO_3 solutions; therefore, the Pa(V) sample could not be prepared in the same way as the actinides used for the first study of multielectron excitations.[12] The formation of Pa(V) polymers can be suppressed in HF and concentrated H_2SO_4 solutions.[13,34]

Recently, the analysis of x-ray absorption near-edge structure and EXAFS spectra of a Pa sample in concentrated sulfuric acid has given evidence of the formation of a mono-oxo ion PaO^{3+} coordinated by five sulfate groups.[27] At high sulfate concentration and a Pa(V) concentration at tracer scale ($c_{Pa} < 10^{-10} M$), the oxo bond disappears.[34] The EXAFS spectrum for Pa(V) sulfate[27] contains a complex fine structure and is therefore not well appropriated to extract multielectron excitation features. It has been shown that these features can be more easily extracted in the absence of the short-bonded oxo groups because they generate a strong scattering contribution extended in the k range far above the occurrence of the multielectron excitation.[12] We used therefore for this study protactinium in its stable oxidation state Pa(V) in aqueous HF solution due to the absence of coordinating oxo groups.

Figure 1 shows the Pa L_3-absorption edge of the sample. The absorption edge has an edge jump $\ln(I_0/I_T)$ of ~ 0.062. Above the edge occurs an intense resonance feature originated from the electron transition of $2p_{3/2}$ core level to $6d$-like molecule orbitals. It has been shown that the $[2p4f]$ double-electron resonance intensity corresponds to the resonance intensity of the $2p$ state; i.e., the stronger the $2p$ resonance is, the more pronounced the $[2p4f]$ resonance is.[12,35] The arrow in Fig. 1 indicates the expected occurrence of the $[2p4f]$ feature with energy E_f. For elements with a low difference between the $2p$ and the $4f$ energies, there appears a strong superposition of the relative high scattering amplitude of $\chi(k)$ and the $[2p4f]$ feature. In such cases, for example, Au $[2p4f]$ with double-electron excitation energy of 110 eV,[8] it was useful to perform a data analysis based on a k weighting of the experimental data. The reported excitation energies of the early actinides are much higher, ranging from 374 eV (Th^{4+}) to 478 eV (Am^{3+}).[12] The intensity of the Th $[2p4p]$ multielectron excitation in relationship to the Th L_3 edge has been determined to $\sim 10^{-3}$.[12] The amplitude of $\chi(k)$ at this energy ($k \sim 10$ Å^{-1}) is already significantly damped; therefore, data weighting with k^3 occurs to be reasonable for visualizing the concerned spectral feature.

The F^- ions form a rather spherical coordination sphere around protactinium, which leads to a sinelike EXAFS oscillation supporting the differentiation of the $[2p4f]$ double-electron excitation from the $2p_{3/2}$ single-electron excitation channel. The Pa(V) fluoride coordination has been identified as PaF_7^{2-} ion previously.[27] The data quality of this study has been improved here by using the transmission mode to collect the x-ray absorption spectrum.

Figure 2 shows the k^3-weighted EXAFS spectrum of Pa^{5+} fluoride together with the spectra of both the neighboring elements thorium and uranium, taken from Ref. 12. The $[2p4f]$ double-electron excitations are indicated by arrows. A systematic shift of the k value already indicates qualitatively a monotonic increase in the $[2p4f]$ excitation energy. The spectra of thorium and uranium are observed from Th^{4+} and U^{4+} hydrates. Their $\chi(k)$ is different from that of Pa^{5+} fluoride due to differences in the coordination and interatomic distances to the ligands. To indicate the differences, the structural parameters reported for Th^{4+} and U^{4+} hydrates are given together with that of Pa^{5+} fluoride in Table I. The hy-

TABLE I. EXAFS structural parameters for protactinium in aqueous HF solution and the aquoions of the two neighboring elements. N_{ij} is the coordination number, and σ^2 is the Debye–Waller factor. The errors in coordination numbers N are ±15%; S_0^2=0.9.

Ion	Shell	R (Å)	N_{ij}	σ^2 (10^{-2} Å^2)	Ref.
Th^{4+}	Th-O	2.44 ± 0.02	9.8	0.68	1
U^{4+}	U-O	2.41 ± 0.02	8.7	0.70	12
Pa^{5+}	Pa-F[a]	2.16 ± 0.02	7.0	0.50	26
Pa^{5+}	Pa-F[b]	2.13 ± 0.01	7.0	0.32	36
Pa^{5+}	Pa-F	2.12 ± 0.02	6.3	0.44[c]	This work
	Pa-F/O	2.48 ± 0.02	1.6	0.44[c]	

[a]Aqueous solution with 0.5*M* HF
[b]Aqueous solution with 0.05*M* HF.
[c]These Debye–Waller factors were free but linked together during the fit procedure.

drates show Th-O and U-O distances of 2.44 and 2.41 Å, respectively,[12] whereas a typical Pa-F distance reported for a PaF_7^{2-} species is 2.16 Å in 0.5*M* HF (Ref. 27) and 2.13 Å in 0.05*M* HF.[36] The sample from Ref. 36 has been used for the study presented here. The only difference with the previous study is that the present measurement was performed in transmission mode with a stabilized beam intensity. The isolated k^3-weighted EXAFS data of Pa(V) fluoride and their corresponding Fourier transform (FT) is shown in Fig. 3; the fit result is given in Table I. The FT represents a pseudoradial distribution function, where peaks are shifted to lower values of $R+\Delta$ relative to the true near-neighbor distances R. This Δ shift of −0.2 to −0.5 Å depends on the scattering behavior of the electron wave in the atomic potentials and was treated as a variable during the shell fits. The FT is dominated by the backscattering signal from one scattering peak. The attempt to fit this backscattering contribution exclusively with seven F^- ions was not successful here and led to a small remaining oscillation in the residual. To obtain good agreement between the experimental EXAFS data and the shell fit, it was necessary to include a second contribution of light scattering atoms such as fluorine or oxygen. Due to their similar scattering amplitude, oxygen and fluorine cannot be differentiated here. To obtain a reasonable fit result, the Debye–Waller factors σ^2 were linked to be at the same magnitude for both shells. The coordination shell splits into ~6.3 F^- ions in a Pa-F distance of 2.12 Å and 1.6 fluoride or oxygen ions in a distance of 2.48 Å. The difference between the two distances is larger than the resolution of 0.13 Å (according to $\Delta R=\pi/2\Delta k$) and can be therefore considered as significant. However, the observation of this longer Pa-F/O distance indicates a small deviation from the spherical coordination geometry. Hydration, hydrolysis, dimerization, or condensation reactions may compete with the fluoride coordination. Hydrolysis can be excluded because coordinated OH groups would be typically related to a shorter actinide-oxygen distance than that observed here. The condensation reaction of hydroxyl-containing Pa species would generate a linear Pa-O-Pa chain. Comparing with that in other actinides, the Pa-O distance in this linear arrangement should be on the order of 2.2 Å, which is far below the observed distance. The formation of a dimer with two bridging fluoroligands occurs to be possible with regard of the bond lengths in the first coordination shell. Such dimers are typical for actinides and have for example recently observed in aqueous Th(IV) solutions.[37] The crystal structure of K_2PaF_7 can act as reference for a dimer, where Pa is bridged by two fluoride atoms in Pa-F distances of 2.31 and 2.47 Å.[38] On the other hand, a dimer is related to a Pa-Pa scattering contribution, which can be expected in a distance of 3.9–4.1 Å. This peak should be detectable, although above $k\sim10$ Å^{-1} a relatively strong noise level already occurs due to the limited Pa concentration. Analog peaks indicating U(VI) hydrate dimers and trimers in aqueous solution have been obtained under similar experimental conditions.[39] Due to the absence of a Pa-Pa scattering peak, a dimer can be ruled out here. Before Pa(V) reach the complete fluoride coordination, the presence of water molecules in the first coordination sphere becomes more probable due to dynamical exchange with the water solvent. Hydration by a single H_2O molecule is typically related to a actinide-oxygen distance of ~2.50 Å. The observed Pa-O distance of 2.48 Å is therefore most likely related to the presence of one or two water molecules in dynamic equilibrium.

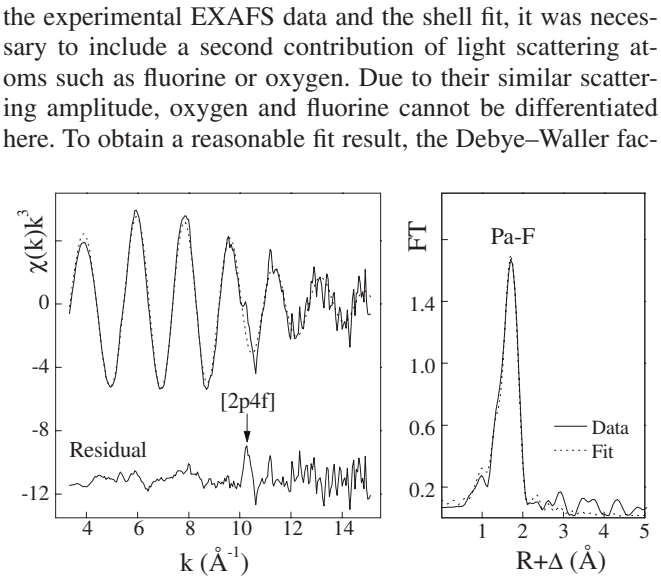

FIG. 3. Pa L_3-edge k^3-weighted EXAFS data (left) and the corresponding Fourier transforms (right) of Pa(V) fluoride.

B. Experimental evidence for [2*p*4*f*] double-electron excitation

The structural contribution has been subtracted from the entire data set to extract the multielectron effect. The difference between the experimental data and the curve fit results in the residual is shown in Fig. 3. This residual represents the experimental noise with increasing amplitude as well as small deviations between the curve fit and the true EXAFS backscattering signal and discontinuities in the atomic background. The strong feature with a peak maximum at k ~10.2 Å^{-1} results from the [2*p*4*f*] double-electron excitation. The energy of the resonance, E_f, is related to the photoelectron wave vector k according to

$$k \sim \sqrt{\frac{2m}{\hbar^2}(E_f - E_0)}, \tag{3}$$

where m is the electron mass and E_0 is the ionization energy. The estimation of E_0 has some uncertainties due to the su-

TABLE II. Experimental energies: E_{1st}—L_3-edge energy approximated by the first derivative of the absorption edge; E_{WL}—energy of the first high absorption maximum (white line); E_f—experimental value of the double-electron excitation (uncorrected for the $2p$ electron energy); E_S—energy of the double-electron excitation.

	Energy (eV)
E_{1st}	16 737.7
E_{WL}	16 741.8
E_f	17 137.9
E_S	396.1

perposition of the electron transitions from $2p_{3/2}$ core level to $6d$-like molecule orbitals. Among the previously discussed procedures to determine E_0 experimentally,[12] the use of the first maximum of the derivative of the raising L_3-absorption edge, E_{1st}, is the most common one. The energy of E_{1st}, extracted from the Pa L_3 edge, is 16 737.7 eV (Table II). The determination of E_S from the difference between E_f and E_0 requires a further correction considering that E_f represents the electron transition into localized final states above the ionization energy. We assume that the energy difference between the ionization energy and the final states of the $[2p4f]$ excitation is similar to that of the $2p_{3/2}$ electron. The energy difference can be therefore approximated from the difference between the final states represented by the white line energy E_{WL} and the ionization energy E_0, represented by E_{1st}. The value of $\Delta E_{WL\text{-}1st}$, extracted from the $4f_{5/2}$ edge of Pa(V), is 4.1 eV. The $[2p4f]$ multielectron excitation energy E_S can be approximated according to

$$E_S = E_f - E_{1st} - \Delta E_{WL\text{-}1st}. \quad (4)$$

The resulting value of E_S is 396.1 ± 10 eV. The $[2p4f]$ energy E_S can be compared with the $4f_{5/2}$ and $4f_{7/2}$ energies within the frame of the $Z+1$ approximation by using the tabulated binding energies from Porter and Friedman.[40] The resulting values are 389 and 379 eV for the $4f_{5/2}$ and $4f_{7/2}$ energy levels, respectively. The experimental value E_S is significantly above the average of the theoretical values. This appears to be reasonable because there is an expected energy difference between the free atom Pa(0), used in the theoretical estimation and Pa(V), used in the experiment. An energy shift of $\sim 1-2$ eV for each additional valence electron has been observed in experiments at the L_3 edge of several actinides.[41] Furthermore, the splitting between the $4f_{5/2}$ and the $4f_{7/2}$ states has not been observed in the experiment. The natural line width Γ_i of the $2p_{3/2}$ level of Pa is 7.3 eV.[42]

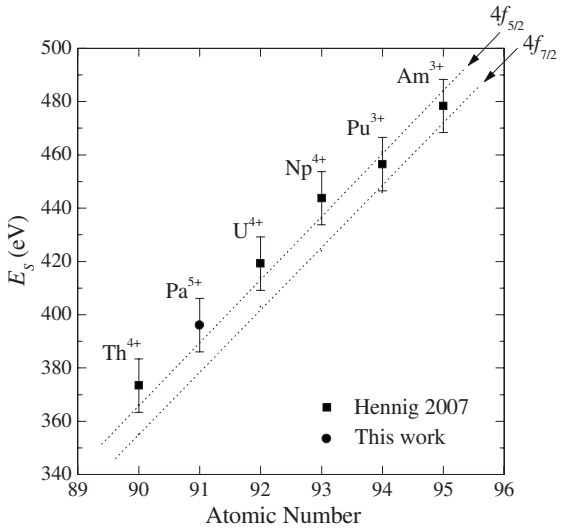

FIG. 4. Experimental energy E_S in comparison with the theoretical $Z+1$ $4f_{5/2}$ and $4f_{7/2}$ energies of the actinides with oxidation state 0. The error bars represent absolute errors, while the relative errors are in the dimension of the data points.

Considering an additional broadening due to the double core hole and the experimental function, it is clear that the j energy splitting of the $4f_{5/2}$ and $4f_{7/2}$ electrons with ~ 10 eV is too small to be resolved. Figure 4 shows a comparison of the experimental observed values E_S of the early actinides and the $4f_{5/2}$ and $4f_{7/2}$ energies according to the $Z+1$ model. This figure indicates a monotonic increase in E_S. The sharp edge-like structure of the multielectron excitation is an indicator for a shake-up channel. Whether there also exists a shake-off channel cannot be clarified from the experiment because the EXAFS scattering contribution is still too strong and circumvents a more sensitive extraction of the atomic background. In a sample of vaporized Hg with a strongly reduced EXAFS amplitude, it was possible to identify both shake-up and shake-off channels for the $[2p4f]$ double-electron excitation at the L edges.[11] The $[2p4f]$ double-electron resonance of the actinides is sharper than for elements with Z values of 79–83. This might be related to the stronger localization of the $4f$ electron level in the case of actinides. A peak broadening as function of increasing Z number, as observed for the $[2p4d]$ double-electron excitation of the lanthanides,[43] could not be observed for the actinides.

ACKNOWLEDGMENTS

This work was supported by the European Actinet Network JRP07–20 "Physico-chemical and redox properties of protactinium."

[1] M. Deutsch and P. Kizler, Phys. Rev. A **45**, 2112 (1992).
[2] R. D. Deslattes, R. E. LaVilla, P. L. Cowan, and A. Henins, Phys. Rev. A **27**, 923 (1983).
[3] E. Bernieri and E. Burattini, Phys. Rev. A **35**, 3322 (1987).
[4] A. Kodre, L. Arčon, J. Padežnik Gomilšek, R. Prešeren, and R. Frahm, J. Phys. B **35**, 3497 (2002).
[5] J. P. Gomilšek, A. Kodre, I. Arčon, and R. Prešeren, Phys. Rev. A **64**, 022508 (2001).

[6] P. D'Angelo, P.-E. Petit, and N. V. Pavel, J. Phys. Chem. B **108**, 11857 (2004).
[7] A. Filipponi and A. Di Cicco, Phys. Rev. A **52**, 1072 (1995).
[8] R. E. Benfield, A. Filipponi, D. T. Bowron, R. J. Newport, and S. J. Gurman, J. Phys.: Condens. Matter **6**, 8429 (1994).
[9] A. Di Cicco and A. Filipponi, Phys. Rev. B **49**, 12564 (1994).
[10] G. Li, F. Bridges, and G. S. Brown, Phys. Rev. Lett. **68**, 1609 (1992).
[11] A. Filipponi, L. Ottaviano, and T. A. Tyson, Phys. Rev. A **48**, 2098 (1993).
[12] C. Hennig, Phys. Rev. B **75**, 035120 (2007).
[13] B. F. Myasoedov, H. W. Kirby, and I. G. Tananaev, in *The Chemistry of the Actinide and Transactinide Elements*, edited by L. R. Morss, N. M. Edelstein, and J. Fuger (Springer, Dordrecht, The Netherlands, 2006), Vol. 1, Chap. 4, p. 161.
[14] W. M. Sackett, Science **132**, 1761 (1960).
[15] J. F. McManus, R. Francols, J.-L. Gherardi, L. D. Keigwin, and S. Brown-Leger, Nature (London) **428**, 834 (2004).
[16] O. Göhring, Phys. Z. **15**, 642 (1914).
[17] O. Hahn, Ber. Dtsch. Chem. Ges. B **54**, 1131 (1921).
[18] O. Hahn and L. Meitner, Phys. Z. **19**, 208 (1918).
[19] F. Soddy and J. A. Cranston, Proc. R. Soc. London, Ser. A **94**, 384 (1918).
[20] D. Brown, J. F. Easy, and C. E. F. Rickard, J. Chem. Soc. A **1969**, 1161.
[21] N. B. Mikheev, A. N. Kamenskaya, I. A. Rumer, S. A. Kulyukhin, and L. N. Auerman, Radiochemistry (Moscow, Russ. Fed.) **35**, 512 (1993).
[22] V. Scherer, F. Weigel, and M. Van Ghemen, Inorg. Nucl. Chem. Lett. **3**, 589 (1967).
[23] N. Edelstein, J. C. Krupa, R. C. Naik, K. Rajnak, B. Whittaker, and D. Brown, Inorg. Chem. **27**, 3186 (1988).
[24] D. Brown and R. G. Wilkins, J. Chem. Soc. **1961**, 3804.
[25] C. M. Marquardt, P. J. Panack, C. Apostolidis, A. Morgenstern, C. Walther, R. Klenze, and T. Fanghänel, Radiochim. Acta **92**, 445 (2004).
[26] R. G. Denning, J. Phys. Chem. A **111**, 4125 (2007).
[27] C. Le Naour, D. Trubert, M. V. Di Giandomenico, C. Fillaux, C. Den Auwer, P. Moisy, and C. Hennig, Inorg. Chem. **44**, 9542 (2005).
[28] T. Toraishi, T. Tsuneda, and S. Tanaka, J. Phys. Chem. A **110**, 13303 (2006).
[29] W. Matz, N. Schell, G. Bernhard, F. Prokert, T. Reich, J. Claußner, W. Oehme, R. Schlenk, S. Dienel, H. Funke, F. Eichhorn, M. Betzl, D. Pröhl, U. Strauch, G. Hüttig, H. Krug, W. Neumann, V. Brendler, P. Reichel, M. A. Denecke, and H. Nitsche, J. Synchrotron Radiat. **6**, 1076 (1999).
[30] T. Ressler, J. Synchrotron Radiat. **5**, 118 (1998).
[31] G. N. George and I. J. Pickering, *A Suite of Computer Programs for Analysis of X-Ray Absorption Spectra* (Stanford Synchrotron Laboratory, Stanford, 2000).
[32] A. L. Ankudinov, B. Ravel, J. J. Rehr, and S. D. Conradson, Phys. Rev. B **58**, 7565 (1998).
[33] C. Keller, Angew. Chem., Int. Ed. Engl. **5**, 23 (1966).
[34] R. Guillaumont, G. Bouissières, and R. Muxart, Actinides Rev. **1**, 135 (1968).
[35] J. Padežnik Gomilšek, A. Kodre, N. Bukovec, and I. K. Škofic, Acta Chim. Slov. **51**, 23 (2004).
[36] M. V. Di Giandomenico, C. Le Naour, E. Simoni, D. Guillaumont, Ph. Moisy, C. Hennig, S. D. Conradson, and C. Den Auwer, Radiochim. Acta (to be published).
[37] R. E. Wilson, S. Skanthakumar, G. Sigmon, P. C. Burns, and L. Soderholm, Inorg. Chem. **46**, 2368 (2007).
[38] D. Brown, S. F. A. Kettle, and A. J. Smith, J. Chem. Soc. A **1967**, 1429.
[39] S. Tsushima, A. Rossberg, A. Ikeda, K. Müller, and A. C. Scheinost, Inorg. Chem. **46**, 10819 (2007).
[40] F. T. Porter and M. S. Freedman, J. Phys. Chem. Ref. Data **7**, 1267 (1978).
[41] T. Reich, G. Bernhard, G. Geipel, H. Funke, C. Hennig, A. Rossberg, W. Matz, N. Schell, and H. Nitsche, Radiochim. Acta **88**, 633 (2000).
[42] M. O. Kraus and J. H. Oliver, J. Phys. Chem. Ref. Data **8**, 329 (1979).
[43] J. A. Solera, J. García, and M. G. Proietti, Phys. Rev. B **51**, 2678 (1995).